RESEARCH ARTICLE

Northern elephant seals adjust gliding and stroking patterns with changes in buoyancy: validation of at-sea metrics of body density

Kagari Aoki[1,2], Yuuki Y. Watanabe[3], Daniel E. Crocker[4], Patrick W. Robinson[5], Martin Biuw[1,6],
Daniel P. Costa[5], Nobuyuki Miyazaki[7], Mike A. Fedak[1] and Patrick J. O. Miller[1,*]

[1]Sea Mammal Research Unit, Scottish Oceans Institute, University of Saint Andrews, Saint Andrews, Fife KY16 8LB, UK,
[2]International Coastal Research Centre, Atmosphere and Ocean Research Institute, The University of Tokyo, 2-106-1 Akahama,
Otsuchi, Iwate 028-1102, Japan, [3]National Institute of Polar Research, 10-3, Midoricho, Tachikawa, Tokyo 190-8518, Japan,
[4]Department of Biology, Sonoma State University, Rohnert Park, CA 94928, USA, [5]Long Marine Laboratory, Department of Ecology
and Evolutionary Biology, University of California, Santa Cruz, CA 95064, USA, [6]Norwegian Polar Institute, Polar Environmental
Centre, 9296 Tromsø, Norway and [7]Center for International Cooperation, Ocean Research Institute, The University of Tokyo,
1-15-1 Minamidai, Nakano-ku, Tokyo 164-8639, Japan

*Author for correspondence (pm29@st-andrews.ac.uk)

SUMMARY

Many diving animals undergo substantial changes in their body density that are the result of changes in lipid content over their annual fasting cycle. Because the size of the lipid stores reflects an integration of foraging effort (energy expenditure) and foraging success (energy assimilation), measuring body density is a good way to track net resource acquisition of free-ranging animals while at sea. Here, we experimentally altered the body density and mass of three free-ranging elephant seals by remotely detaching weights and floats while monitoring their swimming speed, depth and three-axis acceleration with a high-resolution data logger. Cross-validation of three methods for estimating body density from hydrodynamic gliding performance of freely diving animals showed strong positive correlation with body density estimates obtained from isotope dilution body composition analysis over density ranges of 1015 to 1060 kg m^{-3}. All three hydrodynamic models were within 1% of, but slightly greater than, body density measurements determined by isotope dilution, and therefore have the potential to track changes in body condition of a wide range of freely diving animals. Gliding during ascent and descent clearly increased and stroke rate decreased when buoyancy manipulations aided the direction of vertical transit, but ascent and descent speed were largely unchanged. The seals adjusted stroking intensity to maintain swim speed within a narrow range, despite changes in buoyancy. During active swimming, all three seals increased the amplitude of lateral body accelerations and two of the seals altered stroke frequency in response to the need to produce thrust required to overcome combined drag and buoyancy forces.

Supplementary material available online at http://jeb.biologists.org/cgi/content/full/214/17/2973/DC1

INTRODUCTION

Many marine divers, such as phocid seals, undergo substantial changes in body mass and condition as they mature as well as over their annual fasting and foraging cycles (Crocker et al., 1997; Biuw et al., 2003). In capital breeding phocids, resources used during fasting periods associated with breeding and moult are replenished while animals feed at sea between these fasting periods (Costa, 1993). The size of the stores reflects an integration of foraging effort (energy expenditure) and foraging success (energy assimilation). For seals that breed on land, researchers have been able to quantify the consequences of variation in these resources on future survival and reproductive success (Arnbom et al., 1993; Costa, 1993; Fedak et al., 1996; Arnbom et al., 1997; Pomeroy et al., 1999; McMahon et al., 2000; Crocker et al., 2001b; Hall et al., 2001). This has traditionally been accomplished by measuring animal mass combined with determination of water content using isotope dilution techniques (Pace and Rathbun, 1945; Reilly and Fedak, 1990; Arnould, 1995; Bowen and Iverson, 1998). If such measurements are obtained prior to departure from and again upon return to land,

these approaches are extremely useful for determining the net acquired resources integrated over the entire feeding period at sea, and the resources available for onshore process such as breeding and moult. Similarly, if measurements are again obtained prior to the next departure, they permit estimation of the resource utilization of these processes over the time spent on land (Anderson et al., 1993; Costa, 1993). However, these methods cannot be used to map where and when animals are gaining or losing resources as they cannot be applied to free-ranging animals at sea.

Measurements of resource acquisition by animals while at sea are important for understanding how they manage their energy budgets to cover various life history requirements associated with growth and reproduction. But these measurements are also important more generally for understanding foraging ecology and ecosystem interactions, and for management decisions regarding marine species and ecosystems. There are a variety of approaches to estimate where and when marine animals are likely to be feeding, ranging from measurements derived from surface tracks [i.e. transit rate first passage time, fractal landscape, state space models (Fauchald and

Tveraa, 2003; Jonsen et al., 2005; Tremblay et al., 2007; Patterson et al., 2008)] to variations in the diving pattern (Mori, 1998; Bailleul et al., 2008). However, none of these methods provide a measure of food intake and, depending on the animals' foraging strategies and movement patterns, they may miss or over-represent foraging (Robinson et al., 2010). Methods using a variety of sensors to measure actual food intake or prey capture events have also been developed (e.g. Wilson et al., 1992; Austin et al., 2006; Robinson et al., 2007; Kuhn et al., 2008; Suzuki et al., 2009). Although these methods are quite useful to provide timing of feeding and prey encounter rates, they do not quantify resource acquisition, which is represented as the balance between energetic expenditure and energetic intake from prey ingestion.

One alternative approach to estimating foraging success of seals while at sea is based on monitoring changes in their body density as a proxy for lipid content (Crocker et al., 1997; Webb et al., 1998; Biuw et al., 2003), and this approach provides a means to identify advantageous foraging locations (Biuw et al., 2007; Robinson et al., 2010). The rationale behind this approach is that lipid, the main energy reserve in seals, is less dense than seawater whereas non-lipid compartments are slightly more dense than seawater (Moya-Laraño et al., 2008), and changes in relative body composition will therefore influence overall body density and thereby the total forces acting on a diving animal (Fedak et al., 1994; Crocker et al., 1997; Webb et al., 1998; Biuw et al., 2003). Commonly, the term 'buoyancy' is used to refer to the net immersed weight of a body (Beck et al., 2000; Williams et al., 2000) (see Eqn 7). Buoyancy acts vertically, adding to (or subtracting from) drag forces during transit to and from depth (Webb et al., 1998; Beck et al., 2000), and can exceed drag forces at typical travel speeds for many divers. Buoyancy forces have been shown to influence the stroking patterns of swimmers, with increased gliding when buoyancy aids movement (Skrovan et al., 1999; Williams et al., 2000; Miller et al., 2004). Buoyancy forces also modulate the rate of drift during inactive drifting periods (Crocker et al., 1997; Webb et al., 1998; Biuw et al., 2003) and prolonged glides, with higher speeds obtained when buoyancy aids the glide (Watanabe et al., 2006). In stroke-and-glide swimming, buoyancy alters the rate of deceleration (or acceleration) during gliding phases (Miller et al., 2004).

Because of buoyancy's effect on gliding performance, tissue density of a wide range of diving animals (including seals and whales) can potentially be estimated from hydrodynamic analysis of terminal drift (Biuw et al., 2003) or terminal glide speeds (Watanabe et al., 2006), as well as deceleration (or acceleration) rates during glides (Miller et al., 2004). One caveat associated with the use of body density to track changes in foraging success is that it can only be used to estimate changes in the relative body composition, whereas in reality body changes associated with feeding or non-feeding will also change the overall body mass of the animal. It is also possible that resources acquired while feeding are allocated to lean tissue growth rather than the accumulation of lipid energy reserves, leading to an increase in body density. Measuring changes of body mass of freely diving animals would be helpful, but is likely to be more challenging than measuring changes in body density. However, an observed decrease in body density most likely represents the accumulation of lipid reserves, and should therefore provide a conservative indicator of foraging success.

There is also substantial interest in how animals alter their patterns of gliding and active swimming in response to changes in buoyancy. Some longer-term changes in ascent and descent rates appear to correlate with fat content (Webb et al., 1998; Beck et al., 2000). Extensive use of gliding indicates that animals modulate their overall glide and stroke patterns in order to maintain a preferred ascent or descent speed (Thompson et al., 1993) on a dive-by-dive basis. Another factor is that propulsive efficiency of thrusting organs are thought be greatest within a narrow range of Strouhal numbers (fD/U; where f is stroke frequency, D is stroke amplitude and U is forward speed) (Taylor et al., 2003). Thus, animals may have particular biomechanical strategies to maintain propulsive efficiency in changing conditions. During active thrusting periods, the amount of thrust generated could be modulated by altering stroke frequency (Lovvorn et al., 1999; Lovvorn et al., 2004) – defined as the oscillation rate of thrusting during active swimming – stroke amplitude and/or flipper speed (Fish, 1993). In fact, flipper speed and/or stroke amplitude may be fundamentally linked to stroke cycle duration. Though some captive studies have suggested that seals alter stroke cycle frequency rather than amplitude (e.g. Fish, 1988), others have reported that stroke amplitude variations are also important (e.g. Wilson and Liebsch, 2003).

In this study, we experimentally manipulated the body density and mass of instrumented free-diving Northern elephant seals, *Mirounga angustirostris* (Gill 1866), to explore from both an ecological and biomechanical perspective how gliding and stroking patterns are altered by changes in buoyancy forces acting on them. Weights, and in one case a weight and a float, were sequentially released from translocated Northern elephant seals (Oliver et al., 1998) during their return to Anõ Nuevo State Reserve (San Mateo County, CA, USA). These different density and mass manipulation conditions encompassed a wide range of body densities of ecological relevance. We describe how the different density conditions relate to time spent gliding, descent and ascent transit speeds, lateral stroke cycle frequency and lateral dynamic acceleration during ascent and descent. During stroking, we estimate thrust produced by combining drag and buoyancy forces, and relate the thrust to stroke cycle frequency and amplitude of lateral dynamic acceleration. Though it is difficult to measure stroke amplitude directly in free-diving animals, accelerometers record dynamic acceleration of the body, which is oscillated laterally when seals produce thrust (Sato et al., 2003). The amplitude of dynamic body acceleration has been shown to relate to metabolic rate in a diving seabird (Wilson et al., 2006). However, it remains unclear precisely how the amplitude of acceleration might relate to the amplitude of stroking or flipper speed throughout a stroke. We consider that the amplitude of lateral acceleration should be an indicator of thrusting intensity, possibly also reflecting stroke amplitude.

An important goal of our study is to cross-validate three published methods for directly estimating body density from hydrodynamic gliding performance: terminal drift rate (Biuw et al., 2003), deceleration during glides (Miller et al., 2004) and terminal gliding speed (Watanabe et al., 2006). We will also compare the estimates from these methods with body density calculated using the isotope dilution method. The hydrodynamic performance methods have separately been shown to work with different free-ranging species (Biuw et al., 2003; Miller et al., 2004; Watanabe et al., 2006), but have not been evaluated from the same data set on the same species. This set of hydrodynamic gliding methods to estimate body density can be applied to a wide range of diving species and opens new avenues to track the body condition of free-ranging animals and to determine where and when they gain resources.

MATERIALS AND METHODS
Field experiments
We captured four juvenile elephant seals at Anõ Nuevo State Reserve during April 2008. Animals were chemically immobilized using

standard protocols (Le Boeuf et al., 1988; Le Boeuf et al., 2000) and transported to Long Marine Laboratory (Santa Cruz, CA, USA) where they were held overnight for measurement, sample collection and instrument attachment. Body mass, maximum girth and length (standard length L, i.e. the straight line between the tip of the nose and the tip of the tail) were measured (Table 1). Body condition was measured for each seal using water isotope dilution (see Body density measured from isotope dilution methods). Each multi-sensor data logger (W2000-3MPD3GT; 26 mm diameter, 175 mm length, 140 g in air; Little Leonardo Co., Bunkyo-ku, Tokyo, Japan), weight and float was attached to the fur on the back of the seal using nylon mesh and Loctite® Quick Set™ Epoxy (for details see Experimental manipulation of body density). The logger was set to record depth, swim speed and temperature at 1 s intervals, and three-dimensional accelerations (for detecting pitch and hind flipper movements) at 1/16 s intervals, with a memory of 512 Mb. The measurement range of the depth sensor of the data logger was 0–2000 m with a resolution of 0.5 m. The seals were then transported by boat to a release site above the Monterey submarine canyon (36.6°N, 122.5°W), approximately 45 km southwest of Año Nuevo State Reserve. The three seals (seals 1, 2 and 4) returned to the Año Nuevo colony within 2 days and their instruments were recovered (Table 1). We could not recapture one of the seals (seal 3) and did not recover the instrument.

Experimental manipulation of body density

We experimentally changed the body density of our animals by attaching a cuboid weight (3.63 kg in air) and a round float (2.28 kg in air) just behind the data logger on the seal's back. The float was covered with a streamlined plastic housing to provide a consistent alteration in frontal area for each seal. The volume of the float was adjusted so that the float and the weight together were neutrally buoyant in seawater. For seals 1 and 4, we used a time-scheduled release mechanism (Little Leonardo Co.) to automatically release the weight and float 8 and 16 h after deployment, respectively. The release order was switched for seal 2, so the float and then weight were scheduled to be automatically detached 8 and 16 h after deployment, respectively. This allowed us to obtain three buoyancy manipulation conditions: floated-and-weighted (float and weight attached), weighted (only weight attached) and floated (only float attached).

Body density measured with gravity-based isotope dilution methods

We estimated the body composition prior to the release of each seal by isotope dilution. Each animal was given an intraperitoneal injection of ~7.4 MBq of tritiated water (^{3}HHO). After a minimum of 3 h equilibration, a blood sample was taken to determine the specific activity of body water (Costa et al., 1986; Costa, 1987). Injection syringes were gravimetrically calibrated to determine precise injection volumes. Serum samples were collected using freeze trap distillation and counted in 7 ml Betaphase scintillation

cocktail on a Beckmann LS6500 scintillation counter (Ortiz et al., 1978). Total body water (TBW; kg) was calculated from the isotopic dilution space (^{3}HHOspace) using the equation developed for grey seals (Reilly and Fedak, 1990):

$$TBW = -0.234 + 0.971(^3\text{HHOspace}). \qquad (1)$$

The proportion of the total amount of lipid (%TBL) and protein (%TBP) to body mass (kg) and total body ash (TBA; kg) were also calculated (Reilly and Fedak, 1990):

$$\%TBL = 105.1 - 1.47(\%TBW), \qquad (2)$$

$$\%TBP = 0.42(\%TBW) - 4.75, \qquad (3)$$

$$TBA = 0.1 - 0.008 m_{\text{seal}} + 0.05 TBW, \qquad (4)$$

where m_{seal} is the body mass of the seal and %TBW is the proportion of TBW to body mass (kg). Total body density of the seal (ρ_{seal}) was calculated from the proportion (P) and the density (ρ) of each component following Biuw et al. (Biuw et al., 2003):

$$\rho_{\text{seal}} = \rho_l P_l + \rho_p P_p + \rho_a P_a + \rho_{\text{bw}} P_{\text{bw}}, \qquad (5)$$

where the subscripts l, p, a and bw refer to lipid, protein, ash and body water, respectively. We used the following density values: ρ_l=900.7, ρ_p=1340, ρ_a=2300 and ρ_{bw}=994 kg m^{-3}, which are reported for humans (Moore et al., 1963) (cited from Biuw et al., 2003).

The body density of animals for each buoyancy manipulation condition (i.e. floated-and-weighted, weighted and floated conditions) was calculated as:

$$\rho_{\text{seal, manipulation}} = \frac{m_{\text{seal}} + m_{\text{attachment}}}{V_{\text{seal}} + V_{\text{attachment}}}, \qquad (6)$$

where the volume of the seal (m^3) is V_{seal}=$m_{\text{seal}}/\rho_{\text{seal}}$, $m_{\text{attachment}}$ (kg) is the mass of a lead weight and/or the float and $V_{\text{attachment}}$ (m^3) is the volume of a lead weight and/or the float.

Time series data analysis for body density models and stroking patterns

Diving data recorded from the data loggers were analyzed using the software IGOR Pro (WaveMetrics Inc., Lake Oswego, OR, USA). The start and end of dives were defined as seals descending below and ascending above a depth of 2 m, respectively. All deep dives (maximum depth >100 m) were divided into three phases: (1) descent phase (from the start of a dive to the first time at which the depth change rate was negative); (2) ascent phase (from the last time at which the depth change rate was positive to the end of the dive); and (3) bottom phase (the time between the end of the descent phase and the beginning of the ascent phase).

Accelerations in three axes (longitudinal, lateral and dorso-ventral) measured by the logger can be broken into components related to the orientation of the animal with respect to gravity (static components) and dynamic accelerations imposed by the flippers'

Table 1. Summary of study animals and experimental body density manipulation

ID[a]	Sex	Length[b] (m)	Body mass (kg)	Girth (m)	Total tagged duration (h)	Experimental manipulation of body density[c]
Seal 1	Female	1.74	161	1.48	38.6	Weighted, unattached
Seal 2	Male	1.75	162	1.46	70.4	Floated-and-weighted, floated, unattached
Seal 4	Unknown	1.89	193	1.56	31.9	Weighted, unattached

[a]Seal 3 was not recaptured and we could not recover the instrument.
[b]Straight line between the tip of the nose and the tip of the tail (standard length).
[c]See Materials and methods for details.

thrust (dynamic components). Lower-frequency gravity-based acceleration of the longitudinal axis was used to calculate the pitch angle of animals (θ) (Sato et al., 2003; Watanabe et al., 2006). This acceleration was extracted from the raw acceleration data using the low-pass filter at 0.50, 0.50 and 0.40 Hz for seals 1, 2 and 4, respectively, using the software IFDL within IGOR Pro. The frequency boundary for the filter was determined for each seal by calculating the power spectral density of the lateral axis acceleration data using a fast Fourier transformation within IGOR Pro. In all cases, the power spectral density showed a clear trough, which is considered to represent the boundary between gravity-based and dynamic acceleration components (Sato et al., 2007). Negative pitch indicates descent whereas positive pitch represents ascent. The pitch was adjusted for possible off-axis placement on the body by using the cumulative value method (Sato et al., 2003). Higher-frequency dynamic acceleration of the lateral axis was obtained by subtracting the low-frequency components from the raw acceleration data to identify individual strokes. The peaks and troughs of the signal with absolute amplitudes greater than a specified threshold were considered to represent individual strokes (Sato et al., 2003). To select the threshold, we made histograms of absolute amplitudes from all peaks and troughs for each seal. This analysis showed a clear boundary between small noise signals and strokes. We defined the boundary as the threshold (1.27, 0.39, 0.59 m s^{-2} for seals 1, 2 and 4, respectively). An entire peak–trough cycle corresponds to a two flipper strokes (i.e. left–right and right–left).

Speed through the water was measured by an external propeller on the data logger. After analyzing acceleration data, the rotation rate (revolutions s^{-1}) of the propeller was converted into swim speed (m s^{-1}) using a calibration line for each seal (Sato et al., 2003). The calibration line was obtained from a linear regression of rotation rate against swim speed (m s^{-1}), which was calculated from averaged rate of vertical depth change divided by the averaged sine of the pitch at 5 s intervals when the averaged sine of the pitch was greater than 0.8 (for details, see Sato et al., 2003). The regression coefficient values were 0.940, 0.877 and 0.966 for seals 1, 2 and 4, respectively. The corresponding swim speed resolution was 0.035, 0.032 and 0.033 m s^{-1} for seals 1, 2 and 4, respectively.

Body density models

The body density of the animals was estimated by using three different hydrodynamic models: a drift-dive model (Biuw et al., 2003), a glide model (Miller et al., 2004) and a prolonged-glide model (Watanabe et al., 2006). All three models quantify the influence of hydrodynamic drag and buoyancy on a passively moving body. Here, buoyancy is defined as the difference between the body density of the animal and that of the surrounding seawater (Lovvorn and Jones, 1991; Beck et al., 2000):

$$F_B = (\rho_{sw} - \rho_{seal})V_{seal}\boldsymbol{g}, \qquad (7)$$

where F_B is buoyancy force (N), ρ_{sw} is the density of seawater (kg m^{-3}) and $\boldsymbol{g}$ is gravity. The drag of the seal during drifts and glides was calculated as:

$$F_D = 0.5C_d\rho_{sw}AU^2, \qquad (8)$$

where F_D is drag force (N), C_d is the drag coefficient, A is frontal or surface area of the seal (m^2) and U is swim speed (m s^{-1}).

Drift-dive model

We selected drift dives based upon the criteria used by previous studies (Biuw et al., 2003; Mitani et al., 2009). Drift dives include a rapid descent phase (U_1) followed by a prolonged phase of slower descent or ascent (U_2), followed by a rapid ascent to the surface (U_3) (see fig. 1 in Biuw et al., 2003). Drift dives were defined as dives where U_2 had no active stroking and constantly low depth change rate (mean <0.5 m s^{-1}), with continuous descent or ascent and continuously low swim speed (mean <0.5 m s^{-1}).

In drift phases (i.e. U_2), the absolute buoyancy force is assumed to equal the drag force at terminal speed (Biuw et al., 2003). Therefore, the theoretical drift rate U_{drift} (m s^{-1}) is calculated as the terminal speed by $F_D = F_B$ during ascending drift phases and $F_D = -F_B$ during descending drift phases. U_{drift} for descending drift phases is shown as:

$$U_{drift} = \sqrt{\frac{(1 - \rho_{sw}/\rho_{seal})m\boldsymbol{g}}{0.5C_{d,s}\rho_{sw}A_S}} , \qquad (9)$$

where m is the total mass of the seal (kg), A_S is surface area (m^2) and $C_{d,s}$ is the drag coefficient based on total surface area (0.69) (Biuw et al., 2003). Total body mass was calculated as $m_{seal}m_e$, where m_e is a multiplier for entrained water adhering to the surface of the seal. The value for m_e was set to 1.06 based on the measure for a prolate spheroid with a fineness ratio of 5.0 (Skrovan et al., 1999; Miller et al., 2004). A_S was calculated based on the assumption that the seal is two opposing cones with a base that corresponds to total girth (modified from Bell et al., 1997). The anterior cone was assumed to have a height corresponding to one-third of the standard length L, whereas the posterior cone had a height of two-thirds of L. We assume that U_{drift} would correspond to the depth change rate (m s^{-1}) during the drift phase. The depth change rate and ρ_{sw} were averaged during the drift phase. ρ_{seal} was estimated for each dive.

Glide model

During glides, acceleration along the swimming path was determined by the difference between drag force (F_D) and buoyancy force (F_B) parallel to the swimming path: $ma = F_B\sin\theta - F_D$ (Miller et al., 2004). The acceleration is therefore given by:

$$a = -\frac{C_{d,f}A_f}{m}0.5\rho_{sw}U^2 + (\rho_{sw}/\rho_{seal} - 1)\boldsymbol{g}\sin\theta , \qquad (10)$$

where a is the acceleration (m s^{-2}) observed during the glide, $C_{d,f}$ is the drag coefficient based on frontal area (see Calculation of C_d for prolonged-glide and glide models) and A_f is the frontal area (m^2) of the seal. A_f was calculated from the girth measurement, assuming that seals are circular in cross-section.

We conducted this analysis for glides selected by the following three criteria. First, we selected glides where absolute pitch, ascending or descending, averaged more than 30 deg, because the effect of buoyancy should be more evident when the magnitude of buoyancy is weighted by more than sin(30 deg) (Watanabe et al., 2006). Second, to select stable glides, we excluded glides that had rapid changes in pitch (greater than the mean ± s.d. change rate during all dives: 7, 4 and 5 deg s^{-1} for seals 1, 2 and 4, respectively) because deceleration would be caused by the animal's movement. Third, glides that had continuous decreasing or increasing changes in swim speed were selected to exclude unstable glides. Acceleration was measured using a linear regression line of speed vs time. θ, ρ_{sw} and U were averaged during each glide period. These analyses were conducted at 5 s intervals. To increase the range of glide speed, prolonged glides were divided into multiple sub-glides at 5 s intervals (Miller et al., 2004). Only data from every 10 s interval were used to reduce potential autocorrelation of the data. ρ_{seal} was determined by non-linear least-squares methods during each attachment condition for each seal.
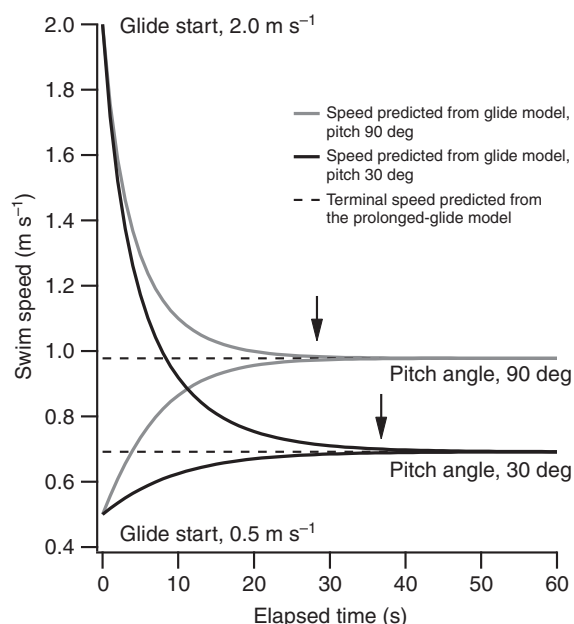
Fig. 1. Example of a simulation to predict the gliding duration that achieves terminal speed during a prolonged glide. Theoretical terminal speed, calculated from the prolonged-glide model, was compared with theoretical speed, calculated from the glide model, for the unattached condition in seal 1. Arrows show the predicted duration needed to reach terminal speed (i.e. the time theoretical speed becomes within 1.0% of theoretical terminal speed). The greatest duration required for the theoretical speed to reach the terminal speed was 36 s.

Prolonged-glide model

In prolonged-glide phases, drag equals the magnitude of buoyancy weighted by $\sin\theta$ at terminal speed: $F_D = F_B \sin\theta$ (Watanabe et al., 2006). The theoretical terminal speed (U_{ter}) is then calculated by:

$$U_{ter} = \sqrt{\frac{(\rho_{sw} / \rho_{seal} - 1)mg\sin\theta}{0.5C_{d,f}\rho_{sw}A_f}} \ . \qquad (11)$$

This equation includes two unknown quantities: ρ_{seal} and U_{ter}. We simulated U_{ter} at various possible ρ_{seal} values within the range 1000–1080 kg m^{-3}, using pitch measured every second. The simulated speed was then compared with the measured speed. ρ_{seal} was determined by least-squares methods for each dive. Similar to the glide model described above, this analysis was conducted for dives where the average absolute value of pitch exceeded 30 deg during descents or ascents, which included prolonged glides.

For this analysis, we predicted the gliding duration required for each individual to achieve terminal speed (Fig. 1) because swim speed at the beginning of a prolonged-glide may not represent the terminal speed (Watanabe et al., 2006). This simulation was conducted based on our analyzing criteria ($|\theta|$>30 deg) and the body density estimated from isotope dilution method (Table 2). First, we calculated theoretical terminal speed from Eqn 11. Second, we simulated changes in swim speed from glide start speed to theoretical terminal speed using the glide model. Eqn 10 of the glide model was rewritten as:

$$U_{t+1} = U_t - \frac{C_{d,f}A_f}{m}0.5\rho_{sw}U^2 + (\rho_{sw} / \rho_{seal} - 1)g\sin\theta \ , \quad (12)$$

where U_{t+1} and U_t are swim speeds (m s^{-1}) at times t+1 and t (s), respectively. Glide start speed (U_0) was set as 0.5–2.0 m s^{-1} based

upon our observations of the seals' speeds. U_0 was substituted as U_t to calculate U_1, and then the U_1 was substituted as U_t to calculate U_2 (i.e. U_{t+1}). Therefore, this equation allows us to calculate changes in swim speed from glide start speed at 1 s intervals. Finally, U_{t+1} (t+1 is the predicted time to reach terminal speed) was assumed to be theoretical terminal speed U_{ter} when it was within 1.0% of U_{ter}. This simulation was conducted for each experimental condition for each seal. The predicted time to reach terminal speed ranged from 12 to 36 s for our animals (Fig. 1) and increased with smaller differences in density between the seal and surrounding seawater. We excluded speed data measured at the beginning of the prolonged glide (40 s) because the measured speed might not have reached terminal speed.

The influence of depth for all body density models

The total buoyancy of an air-breathing aquatic animal changes with depth owing to residual air in the lungs. This residual air could affect our estimation of ρ_{seal}, but this effect is reduced at greater depths because air volume decreases with increasing depth following Boyle's law (Biuw et al., 2003). To minimize the effect of gases on buoyancy, we only used data from depths greater than 100 m.

Because buoyancy is a function of the difference between the density of the animal and seawater, changes in seawater density with depth could substantially affect our estimation of ρ_{seal} (see Miller et al., 2004). Therefore, the density of seawater was estimated at 1 s intervals from depth (m) and temperature (°C), measured by the data loggers, and salinity estimates of 34.84‰ (Vogel, 1994) using the International Equation of State of Seawater (UNESCO, 1981). Water temperature at depths greater than 100 m ranged from 5.1 to 10.7°C, and the corresponding density of the seawater ranged between 1027.2 and 1030.8 kg m^{-3}.

Calculation of C_d for prolonged-glide and glide models

Gliding seals should swim head first to maximize their movement efficiency by minimizing drag. Therefore, the drag coefficient during glides would be different from that of drift phases, during which the body orientation is more like a falling leaf (Mitani et al., 2009), for which we used a surface area drag coefficient of 0.69 (Biuw et al., 2003). Drag force during glides was calculated from the deceleration rate during horizontal gliding: $F_D = ma$ (Bilo and Nachtigall, 1980; Williams and Kooyman, 1985; Feldkamp, 1987; Watanabe et al., 2006). $C_{d,f}$ is therefore given by:

$$C_{d,f} = 2m(U_t - U_{t+1}) / (\rho_{sw}A_fU^2), \qquad (13)$$

where U_t and U_{t+1} were averaged to give mean glide speed (U; m s^{-1}); ρ_{sw} was also averaged during these periods. We extracted 50 deceleration phases for each experimental condition of each seal when the seals swam horizontally (i.e. depth changes are zero) using stroke-and-glide patterns during the bottom phases of dives.

Eqn 13 can be rewritten as:

$$\frac{C_{d,f}A_f}{m} = 2(U_t - U_{t+1}) / (\rho_{sw}U^2) \ . \qquad (14)$$

Therefore, by using horizontal glides to estimate the constant on the left-hand side of Eqn 14, it is possible to calculate body density using the prolonged-glide and glide models even without specific information on body mass and reference surface area.

The drag coefficient was recorded along with the Reynolds number (Re): $Re = LU/\nu$, where ν is the kinematic viscosity of seawater (1.35×10^{-6} m^2 s^{-1}) (Lide, 2003). We estimated $C_{d,f}$ at 293±63, 183±102 and 157±55 m for seals 1, 2 and 4, respectively.

Table 2. Comparison of body density estimated from three hydrodynamic models and the body density measured using the isotope dilution method

ID	Condition	$C_{d,f}$[a]	Re ($\times 10^6$)	Drift model Body density (kg m^{-3})	N	Residual[b]	Glide model Body density[c] (kg m^{-3})	N	Residual[b]	Prolonged-glide model Body density (kg m^{-3})	N	Residual[b]	Isotope dilution Body density (kg m^{-3})
Seal 1	Weighted	0.17±0.056	1.6±2.5	1067.9±7.1	4	−7.8	1064.3±1.2***	35	−4.2	1064.4±2.0	12	−4.3	1060.1
	Unattached	0.16±0.047	1.6±2.3	1046.0±2.9	8	−7.1	1043.1±0.4***	120	−4.2	1043.0±1.6	37	−4.1	1038.9
Seal 2	Floated-and-weighted	0.26±0.084	1.1±1.9	–	0	–	1041.5±0.5***	30	−3.3	1040.2±1.0	5	−2.0	1038.2
	Floated	0.23±0.068	1.1±1.4	–	0	–	1014.0±0.3***,d	76	+1.4	1013.1±2.6e	34	+2.3	1015.4
	Unattached	0.19±0.058	1.2±2.0	1038.6±0.5	2	−0.4	1039.4±0.4***	62	−1.2	1040.8±1.0	8	−2.6	1038.2
Seal 4	Weighted	0.21±0.044	1.7±2.8	–	0	–	1060.3±0.8***	43	−2.4	1059.0±2.0	15	−1.1	1057.9
	Unattached	0.20±0.049	1.5±1.0	–	0	–	–	6	–	–	0	–	1040.2
Mean						−5.1			−2.3			−2.1	
s.d.						4.1			2.4			2.7	

[a]Drag coefficient with Re was calculated from horizontal gliding.
[b]The difference calculated by subtracting the body density of the models from that of isotope dilution method.
[c]Estimated values ± s.e. are shown. ***, $P<0.001$.
[d]Estimated value including effects of induced drag (see Appendix), 1017.5±0.1*** (residual=−2.1).
[e]Estimated value including effects of induced drag (see Appendix), 1017.0±0.9 (residual=−1.6).
–, no data.

Because we cannot assume that the seals were neutrally buoyant at these depths, the seals should produce lift to maintain their horizontal motion. We specifically address the potential influence of lift on our analyses in the Appendix.

Stroking patterns

Stroke rate (s^{-1}) during descent and ascent was calculated from the total number of strokes divided by the duration of each phase for each dive. The amplitude of lateral acceleration (m s^{-2}) was considered to be a relative indicator of stroke intensity and was expected to be associated with stroke amplitude (m). The amplitude of lateral acceleration was quantified as half of the peak-to-peak recorded values. Amplitude of lateral acceleration was averaged over each phase for each dive during descent and ascent. These analyses were conducted for all deep dives (maximum depth >100 m)

To investigate the effects of buoyancy in relation to swim speed and stroke patterns, we estimated propulsive force while our animals swam actively. The propulsive force of the animals should equal resistance force (F_R), including drag and buoyancy at times when speed is constant (Lovvorn et al., 2004). The resistance force is calculated by $F_R = \lambda F_D + F_B \sin\theta$ from Eqns 7, 8 and 11. For this analysis, we used the body density calculated using the isotope dilution method. The term λ is the active-to-passive drag ratio. Studies of captive phocid seals and dolphins suggested that actively swimming animals had higher drag than gliding animals (Williams and Kooyman, 1985; Fish, 1988; Fish, 1993). However, hydrodynamic models estimated that active drag was less than the passive drag in several marine animal species (Hind and Gurney, 1997). This conclusion was supported by Barrett et al. (Barrett et al., 1999), who reported that drag in an actively swimming fish robot at an Re of approximately 10^6 can be reduced by 50–70% compared with that in the same robot when passively towed. Simulation of the hydrodynamics of carangiform locomotion also showed that active drag decreased to approximately 75% at high Re and Strouhal numbers (400 and 0.6, respectively), compared with rigid body drag (Borazjani and Sotiropoulos, 2008). Although we do not have any information on the active-to-passive drag ratio of our animals, their Re numbers were usually greater than 10^6 (Table 2). We therefore followed Hind and Gurney (Hind and Gurney, 1997), who reported the optimal λ to be close to 1 for phocid seals. This assumption might cause an underestimation or overestimation of the active drag,

so we carried out a sensitivity analysis by additionally calculating the results using active-to-passive ratios of 0.5 and 2.

We then correlated the estimated propulsive force against the amplitude of lateral acceleration and stroke cycle frequency. Stroke cycle frequency (Hz), which corresponds with stroke cycle duration, was calculated at 1 s intervals using the software Ethographer 1.20 (Sakamoto et al., 2009) in IGOR Pro. We averaged data over 5 s intervals, and only analyzed every 10 s interval to reduce the influence of autocorrelation. This analysis was conducted at depths of more than 100 m at each condition for each seal.

All statistical tests were conducted using the R 2.6.2 package (R Foundation for Statistical Computing, Vienna, Austria). We set statistical significance at $P<0.05$. Data are reported as means ± s.d.

RESULTS

A total of 140.8 h of data, including 314 complete dives (>100 m), were obtained. For seals 1 and 4, the float detached just after release of the seal, rather than at the scheduled detachment time. For seal 2, the float detached after 32 h instead of the 8 h that was programmed (see supplementary material Fig. S1). Because the attachment of the float might have been unstable during the period between the scheduled release at 8 h and the actual release at ~32 h, we evaluated whether the drag coefficient $C_{d,f}$ was different before and after the scheduled release time in the floated-and-weighted condition. However, $C_{d,f}$ was not significantly different between these two periods (Mann–Whitney U-test, $U_{50}=1225$, $P=0.87$; before, 0.25±0.048, $N=50$; after, 0.26±0.110, $N=50$). A total of four different conditions were obtained from the three seals (weighted, floated, floated-and-weighted and unattached conditions; Table 1).

Validation of at-sea metrics of body density

Calculation of body density: drift-dive method

A total of 14 drift dives were observed in the weighted and unattached conditions for seal 1 and the unattached condition for seal 2 (Table 2). In drift phases, these seals gradually descended (drift rate: 0.38±0.033 m s^{-1}, $N=4$ dives and 0.26±0.021 m s^{-1}, $N=8$ dives for weighted and unattached conditions in seal 1, respectively; 0.20±0.005 m s^{-1}, $N=2$ dives for unattached in seal 2). Both seals were in a head-up orientation during drifting (seal 1: +22.7±8.9 deg, $N=4$ dives and +22.5±11.6 deg, $N=8$ dives during the weighted and unattached conditions, respectively; seal 2: +27.9±2.5 deg, $N=2$

dives). The start and end depths of the drift segment (i.e. U_2 phase) were 246±19 and 423±39 m for the weighted condition in seal 1 (N=4 dives), 213±63 and 319±33 m for the unattached condition in seal 1 (N=8 dives), and 298±35 and 368±24 m for the unattached condition in seal 2 (N=2 dives), respectively. The mean duration of drift segments was 428±161 s (N=14 dives).

Drag coefficient for prolonged-glide and glide models
For the glide and prolonged-glide models, we used the value of $C_{d,f}$ obtained during each attachment condition for each seal to estimate the body density of the animals (Table 2). There were no significant differences in $C_{d,f}$ between the weighted and unattached conditions for seals 1 and 4 (Mann–Whitney U-test, seal 1, U_{50}=1015, P=0.19; seal 4, U_{50}=1033, P=0.23). However, $C_{d,f}$ was significantly different among the three different conditions for seal 2 (Kruskal–Wallis test, χ^2_2=24.6, P<0.001). Seal 2 was the seal to which the float remained attached, and the results suggest that attachment of the float increased the drag coefficient despite the streamlined plastic housing that provided a consistent alteration in frontal area with or without the float.

Calculation of body density: glide method
From the three seals combined, we recorded a total of 372 ascending and descending glides that met the analytical criteria. Insufficient glide data were obtained from the unattached condition for seal 4. The glides had an absolute value of pitch of 47.3±11.9 deg (N=372 glides). Acceleration ranged from –0.093 to 0.083 m s^{-2} and was affected by the animal's speed prior to initiating the glide and its pitch during the glide. The overall range of speed was 0.63 to 1.80 m s^{-1} and varied depending on attachment conditions for each seal (1.19–1.80 and 0.71–1.54 m s^{-1} for the weighted and unattached conditions in seal 1, respectively; 0.69–1.12, 0.63–1.22 and 0.74–1.30 m s^{-1} for the floated-and-weighted, floated and unattached conditions in seal 2, respectively; 1.10–1.61 and 1.06–1.24 m s^{-1} for the weighted and unattached conditions in seal 4, respectively). The mean duration of glides, excluding prolonged glides of more than 1 min, was 17.5±11.1 s (N=46 glides, min. 8 s). Theoretical acceleration from the model corresponded well with observed acceleration when an appropriate value of the body density, obtained by least-squares methods, was used (see Fig. 2 for one example). Model fits of estimated body density were all statistically significant at P<0.001 for all conditions of all seals (Table 2). The absolute value of the mean difference between observed acceleration and predicted acceleration values was 0.0177 m s^{-2}.

Calculation of body density: prolonged-glide method
A total of 111 prolonged glides during ascent and descent meeting the analytic criteria were obtained from the three seals (Table 2). No prolonged glides were observed in the unattached condition in seal 4. Mean absolute pitch of dives used for this analysis was 45.3±7.9 deg (N=111 prolonged glides). After the start of prolonged glides, measured speed gradually decreased and then remained relatively constant thereafter (see Results, Changes in stroking patterns from body density manipulations). When appropriate values of body density obtained by least squares were used, the theoretical speeds corresponded well with the observed speeds (see fig. 6 in Watanabe et al., 2006).

Comparison among three hydrodynamic models
The body densities estimated from all three hydrodynamic models were highly correlated with each other (drift model *vs* prolonged-glide model, r^2=0.949; prolonged-glide model *vs* glide model,
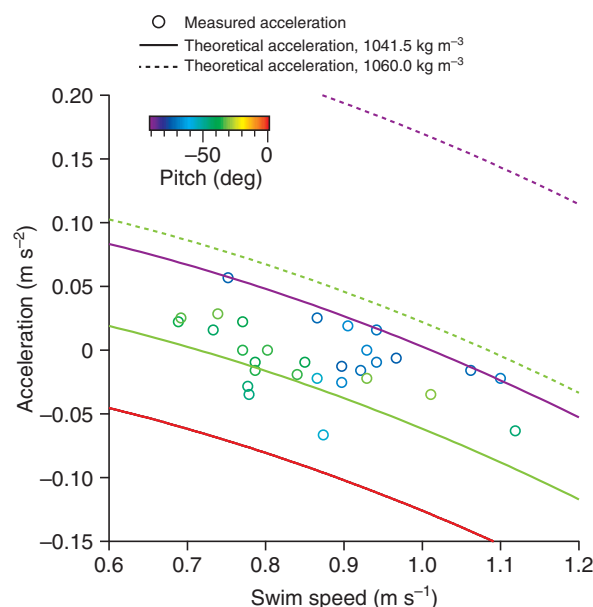

Fig. 2. Example of measured (circles) and theoretical (lines) acceleration *vs* speed and pitch angle. Theoretical acceleration was calculated using the glide model assuming a body density of 1041.5 kg m^{-3} (solid lines) and a body density of 1060.0 kg m^{-3} (dashed lines) for the floated-and-weighted condition in seal 2. The color scale for both lines and circles indicates pitch angle, which is negative during descent.

r^2=0.996; glide model *vs* drift model, r^2=0.977). The body densities estimated from the prolonged-glide model were close to the body densities estimated from the glide model (within ±1.5 kg m^{-3}; Table 2). The differences between the body densities estimated from the drift model and the other two model approaches were somewhat greater; the range of the differences from the glide model and the prolonged-glide model was –0.8–3.6 and –2.2–3.5 kg m^{-3}, respectively (Table 2).

Comparison of body density measured using isotope dilution
Body density calculated with the isotope dilution method was similar among the three seals (range=1038.2–1040.2 kg m^{-3}; unattached condition in Table 2). We combined the body density estimated from isotope dilution in the unattached condition with the effect of the weights and floats to estimate the density of each seal in each attachment condition (Table 2, final column). The estimated densities in the different attachment conditions were highly correlated with body densities estimated from the drift model ($F_{1,1}$=20.5, P<0.001, r^2=0.954), the glide model ($F_{1,4}$=603.3, P<0.001, r^2=0.992) and the prolonged-glide model ($F_{1,4}$=399.9, P<0.001, r^2=0.988; Fig. 3). In most cases, densities estimated with the hydrodynamic models were slightly higher than those estimated using isotope dilution methods (Table 2).

Changes in stroking patterns from body density manipulations
Examples of stroke patterns of all conditions for each seal are shown in Fig. 4. The three primary stroking patterns were observed: prolonged glide, stroke-and-glide and continuous stroking (Sato et al., 2003; Miller et al., 2004; Watanabe et al., 2006). Prolonged glides were marked by extended periods with no active strokes, and a gradual change in swim speed (Fig. 4A–C,E,F). Stroke-and-glide
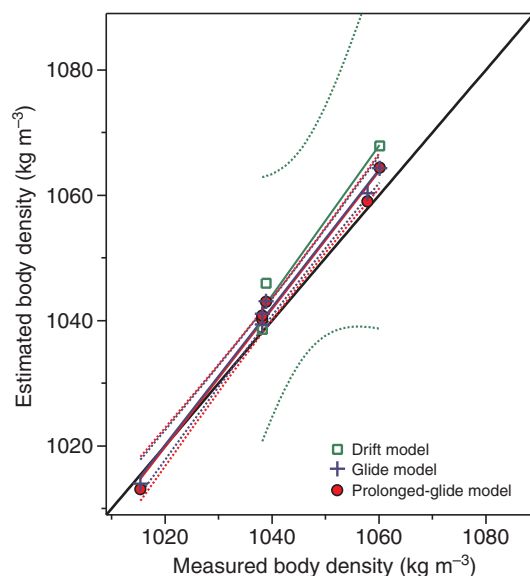
Fig. 3. Correlation between the body density estimated from three hydrodynamic models (drift, glide and prolonged-glide models) at each attachment condition for each individual seal, and the body density measured using the isotope dilution method. The diagonal black line is a 1:1 line. The regression lines are represented by a green line for the drift model, a blue line for the glide model and a red line for the prolonged-glide model. The 90% confidential interval for each model is shown with a dashed line of the same color.

was characterized by intermittent strokes with corresponding oscillations of swim speed (Fig. 4D,E,G). Continuous stroking showed relatively constant speed (Fig. 4A–C,F,G).

Weighted vs unattached conditions in seals 1 and 4

Stroking patterns were similar in both conditions in seal 1, but different between conditions in seal 4. Seal 1 employed prolonged glides during descent (weighted, $N=18$ dives, 90.0% of dives; unattached, $N=54$ dives, 80.6%) and continuous stroking during ascent in both conditions (weighted, $N=20$ dives, 100%; unattached, $N=61$ dives, 97.0%; Fig. 4A,B). Similarly, seal 4 employed prolonged glides during descent ($N=22$ dives, 100%) and continuous stroking during ascent ($N=22$ dives, 100%; Fig. 4C) in the weighted condition. In contrast, seal 4 employed stroke-and-glide at both descent and ascent in the unattached condition (descent, $N=34$ dives, 94.4%; ascent, $N=33$ dives, 91.7%; Fig. 4D). In both seals, the descent stroke rate was lower in the weighted condition than the unattached condition, whereas the ascent stroke rate was higher in the weighted condition than in the unattached condition (Table 3). During ascent, the amplitude of the lateral acceleration was significantly greater in the weighted condition than in the unattached condition in both seals (Table 3).

Floated vs unattached and floated-and-weighted conditions in seal 2

The stroke pattern in the floated condition was clearly different from the other two conditions. During descent, seal 2 employed prolonged glides ($N=33$ dives, 63.4%) for the floated-and-weighted condition, continuous stroking ($N=45$ dives, 100%) for the floated condition and, continuous stroking ($N=25$ dives, 36.2%) or stroke-and-glide ($N=24$ dives, 34.8%) for the unattached condition (Fig. 4E–G). During ascent, this seal displayed stroke-and-glide ($N=41$ dives, 78.8%) for the floated-and-weighted condition, prolonged glides

($N=40$ dives, 88.9%) for the floated condition and continuous stroking ($N=69$ dives, 100%) for the unattached conditions (Fig. 4E–G). During descent, this seal showed a higher stroke rate in the floated condition than in either of the other two conditions, whereas during ascent, a lower stroke rate was observed in the floated condition than in either of the other two conditions (Table 3). The fastest swim speeds were measured in the unattached condition in both descent and ascent (Table 3). The seal exhibited relatively large amplitude of lateral acceleration when it swam against the direction of buoyancy in all three conditions (Table 3).

Adjustment of stroke cycle frequency and amplitude of lateral acceleration in response to changing propulsive force

These analyses were conducted for the weighted and unattached conditions in seals 1 and 4 and the unattached condition in seal 2 because the presence of the float (i.e. floated-and-weighted and floated conditions) altered the drag coefficient and appears to have affected the speed at which seal 2 swam. The optimal speed of swimming animals is expected to be proportional to (basal metabolic rate/drag)$^{1/3}$ (Alexander, 1999; Sato et al., 2010). It is reported that swim speed decreased when drag was experimentally increased in African penguins (Wilson et al., 1986). Thus, the increase of the drag coefficient may have led to the decrease in swim speed for the floated-and-weighted and floated conditions in seal 2. These conditions for seal 2 were not included for this analysis because the drag coefficient and swim speed, which strongly affect the resistance force, were outliers.

The amplitude of lateral acceleration and stroke cycle frequency in relation to the resistance force is shown in Fig. 5. We investigated whether the changes in lateral acceleration amplitude and stroke cycle frequency with resistive force varied between individuals. This statistical model regressed the resistance force as the dependent variable against the amplitude of lateral acceleration, stroke cycle frequency and seal ID as fixed independent factors, and the interaction among these three factors was assessed with F-statistics (Fox, 2002). The three-way interaction was significant ($F_{2,2583}=7.33$, $P<0.001$), indicating that the pattern in which the amplitude of lateral acceleration and stroke cycle frequency varied against resistance force differed between individuals. We therefore regressed resistive force on stroke cycle frequency, the amplitude of lateral acceleration and their interaction separately for each individual (Table 4). The adjusted r^2 of the multiple regression models was high, indicating that much of the variation in force overcome is captured by the two measured variables (seal 1, $r^2=0.887$, $F_{3,1047}=2738$, $P<0.0001$; seal 2, $r^2=0.651$, $F_{3,1057}=666.1$, $P<0.0001$; seal 4, $r^2=0.885$, $F_{3,475}=1230$, $P<0.0001$).

The amplitude of lateral accelerations positively correlated with the resistance force for all seals (see Slope of independent variables in Table 4). The partial correlation coefficient of the amplitude of lateral accelerations was higher than that for stroke cycle frequency for all seals (Table 4). Stroke cycle frequency was positively correlated with resistive force in seals 1 and 2, but not in seal 4 (Table 4). There was a significant interaction term for seal 1, suggesting that changes in stroke cycle frequency and amplitude of lateral accelerations were not made independently by that seal. Running the same analysis using active-to-passive drag ratios of 0.5 and 2.0 did not substantially change how amplitude of lateral acceleration and stroke cycle frequency related to resistive force.

DISCUSSION

By manipulating the body density and mass of seals, we were able to demonstrate that body density can be estimated from changes in
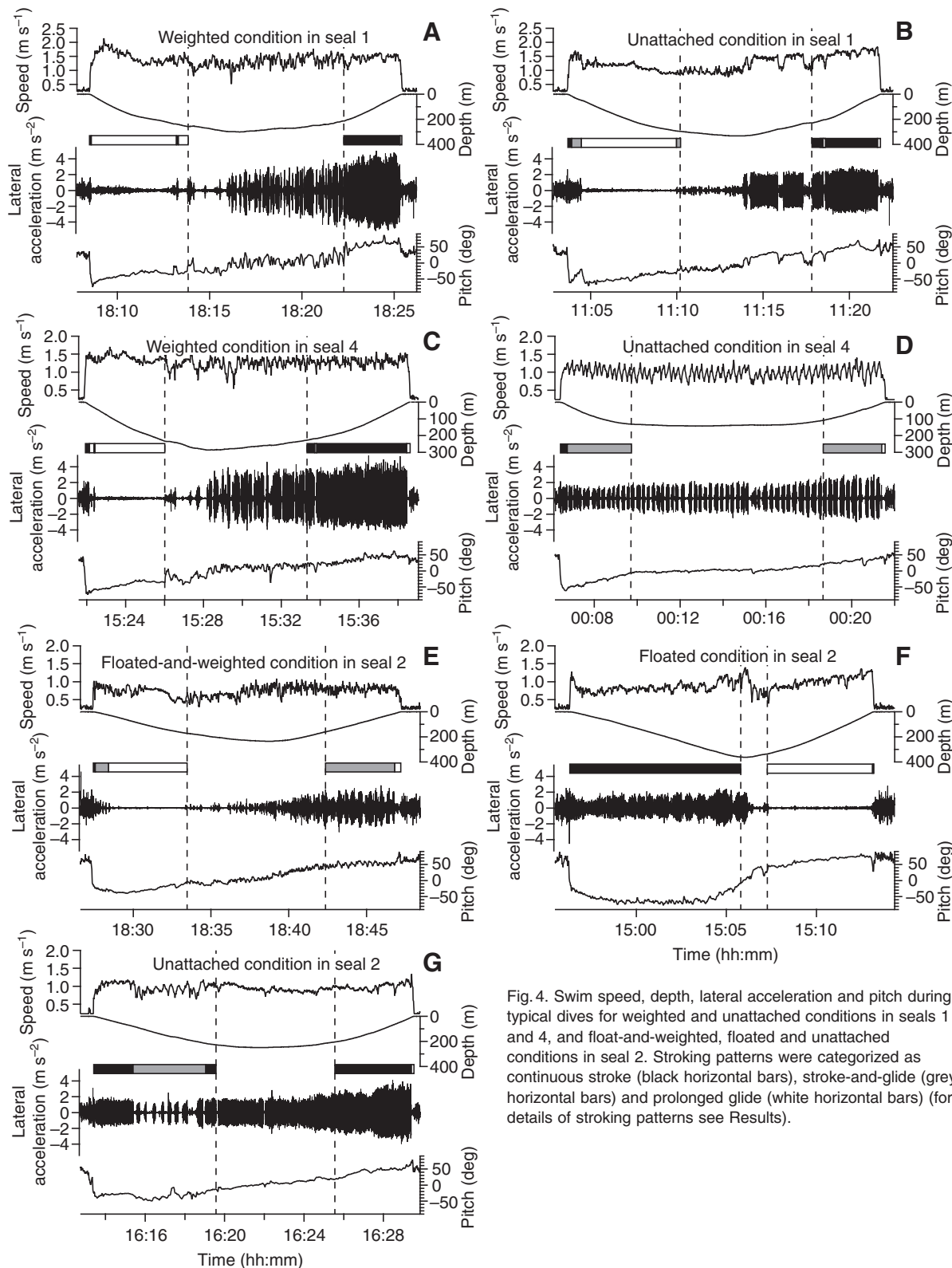
Fig. 4. Swim speed, depth, lateral acceleration and pitch during typical dives for weighted and unattached conditions in seals 1 and 4, and float-and-weighted, floated and unattached conditions in seal 2. Stroking patterns were categorized as continuous stroke (black horizontal bars), stroke-and-glide (grey horizontal bars) and prolonged glide (white horizontal bars) (for details of stroking patterns see Results).

hydrodynamic gliding performance of free-diving animals. The presented methods should provide an approach for measuring and tracking changes in body condition of a wide spectrum of diving species. Because use of the hydrodynamic methods to measure body density does not require capturing animals to make measurements, it may be useful to study body condition of obligate marine divers, such as cetaceans, which are difficult to capture to measure body condition using traditional methods. We also described how the seals modulated their stroking and gliding patterns with changes in buoyancy. The body densities achieved by attaching a lead weight and float ranged from 1015.4 to 1060.1 kg m^{-3} (Table 2). Estimated actual body lipid contents corresponding to these body

Table 3. Comparison of stroking patterns and swim speed among experimental body-density manipulation conditions for each seal

ID	Condition	No. of dives	Dive depth (m)	Pitch (deg) Descent	Pitch (deg) Ascent		Stroke rate[a] (s⁻¹) Descent	Stroke rate[a] (s⁻¹) Ascent		Swim speed[b] (m s⁻¹) Descent	Swim speed[b] (m s⁻¹) Ascent		Amplitude of lateral acceleration[b,c] (m s⁻²) Descent	Amplitude of lateral acceleration[b,c] (m s⁻²) Ascent	
Seal 1	Weighted	20	358±80	−42.2±7.7	47.7±7.9	***	0.10±0.17 ***	1.93±0.13	***	1.51±0.13	1.50±0.12	NS	1.85±0.73 ***	3.98±0.30	***
	Unattached	67	301±91	−44.7±7.7	37.1±7.4		0.24±0.29 ***	1.68±0.19		1.22±0.18	1.54±0.16		1.56±0.17 ***	2.36±0.20	
Seal 2	Floated-and-weighted	52	191±110	−32.5±5.6	37.8±4.7		0.22±0.13 ***	1.31±0.16		0.76±0.06	0.83±0.09		0.71±0.17 ***	1.17±0.34	
	Floated	45	281±102	−48.9±6.2	45.6±6.3	***	1.91±0.09 ***	0.11±0.20	***	0.99±0.11	0.91±0.09	***	1.49±0.25 ***	0.80±0.23	***
	Unattached	69	242±94	−36.0±7.4	36.2±8.3		1.20±0.45 ***	1.78±0.17		1.07±0.13	1.12±0.13		1.25±0.22 ***	2.57±0.35	
Seal 4	Weighted	22	276±67	−42.7±3.8	36.7±6.1	***	0.15±0.05 ***	1.53±0.07	***	1.33±0.07	1.29±0.08	***	1.39±0.15 ***	3.45±0.26	***
	Unattached	36	172±42	−34.5±5.6	30.3±3.9		1.16±0.10 NS	1.13±0.15		1.12±0.05	1.13±0.13		1.38±0.10 ***	2.20±0.19	

[a]Stroke rate was compared among experimental body-density manipulation conditions and between descent and ascent using GLM with Poisson error distribution.
[b]Swim speed and amplitude of lateral acceleration were compared among experimental body-density manipulation conditions using t-test for seals 1 and 4 and one-way ANOVA for seal 2.
[c]Amplitude of lateral acceleration was compared between descent and ascent using t-test.
***, $P<0.001$; NS, not significant.

densities are 25.4–46.4%, as determined by modifying Eqn 5 to $\rho_{seal}=\rho_l P_l+\rho_{lipid\text{-}free}(1-P_l)$, where $\rho_{lipid\text{-}free}$ is calculated from $\rho_p P_p+\rho_a P_a+\rho_{bw}P_{bw}$ (1114.6 kg m⁻³). This range compares well with observed individual variations in lipid content estimated using labeled water (23.1–46.2%) (Biuw et al., 2003), and the dramatic seasonal changes in body lipid content that pinnipeds regularly undergo that often range from <20 to >40% (Crocker, 1995; Fedak et al., 1996; Beck et al., 2000). We discuss our results from both a biomechanical and an ecological perspective.

Validation of at-sea metrics of body density
Hydrodynamic performance vs isotope dilution
The body density estimated from the three hydrodynamic models was highly correlated with that measured using the isotope dilution method, but the densities measured using our models were slightly greater than those estimated from body composition derived from isotope dilution estimates of total body water (Table 2). It is difficult to assess which value is actually more accurate as all of these techniques are indirect measures of body composition and require certain assumptions (Reilly and Fedak, 1990; Arnould et al., 1996; Bowen and Iverson, 1998). However, the variation among the three hydrodynamic models is within 1% of the body density measurements, which means that the variation is within 2% of lipid contents (calculated from modified Eqn 5). Lipid content estimates from isotope dilution could easily vary by 3% lipid (Lukaski, 1987). Given these uncertainties and estimates of

precision, none of the measures were significantly different, and all the hydrodynamic methods provided estimates of body composition of the same order of accuracy as estimates obtained using isotope dilution. It would be useful to have an independent and direct estimate of body density in tested seals, which could theoretically be accomplished using whole-body air-displacement plethysmography (Fields et al., 2005).

Although differences between the estimated body densities using the isotope dilution method and the hydrodynamic models were quite small, it is worth mentioning possible errors in our hydrodynamic body-density analyses. All methods require an estimate of the drag force acting on the body. Biuw et al. pointed out that the drag coefficient is the most important factor in predicted body density for the drift model (Biuw et al., 2003). As they suggested (Biuw et al., 2003), we should not expect the drag coefficient to be constant. The drag coefficient of a diver may be affected by changes in the animal's shape (e.g. girth, fineness ratio) due to gains or losses of lipid. The single value of the drag coefficient used in the drift method might be improved upon by considering how changes in body form might influence the drag coefficient (Vogel, 1994). Additionally, because elephant seals passively descended like a 'falling leaf' during drift dives (Mitani et al., 2009), postural changes against the direction of drift will result in variations in the drag coefficient. Mitani et al. reported that the pitch of animals was close to horizontal (see data supplement in Mitani et al., 2009), whereas our animals showed

Table 4. Multiple regression models describing the effect of stroke cycle frequency and the amplitude of lateral acceleration and their interaction on resistance force

	Seal 1			Seal 2			Seal 4		
		t	P		t	P		t	P
Slope of independent variables									
Stroke cycle frequency	88.2	15.32	<0.0001	19.6	2.37	<0.05	1.8	0.12	0.905
Amplitude of lateral acceleration	26.0	13.06	<0.0001	9.5	2.78	<0.01	12.1	2.04	<0.05
Stroke cycle frequency × Amplitude of lateral acceleration	−11.7	−5.94	<0.0001	1.8	0.50	0.619	11.5	1.59	0.113
Intercept	−71.5	5.27	<0.0001	−21.0	−2.79	<0.01	−13.8	−1.11	0.268
Adjusted R^2 for the full model	0.887			0.651			0.885		
Partial r^2									
Resistance force vs Stroke cycle frequency	0.506			0.212			0.159		
Resistance force vs Amplitude of lateral acceleration	0.791			0.783			0.929		

Partial correlation coefficients were calculated among amplitude of lateral acceleration, stroke cycle frequency and the resistance force.
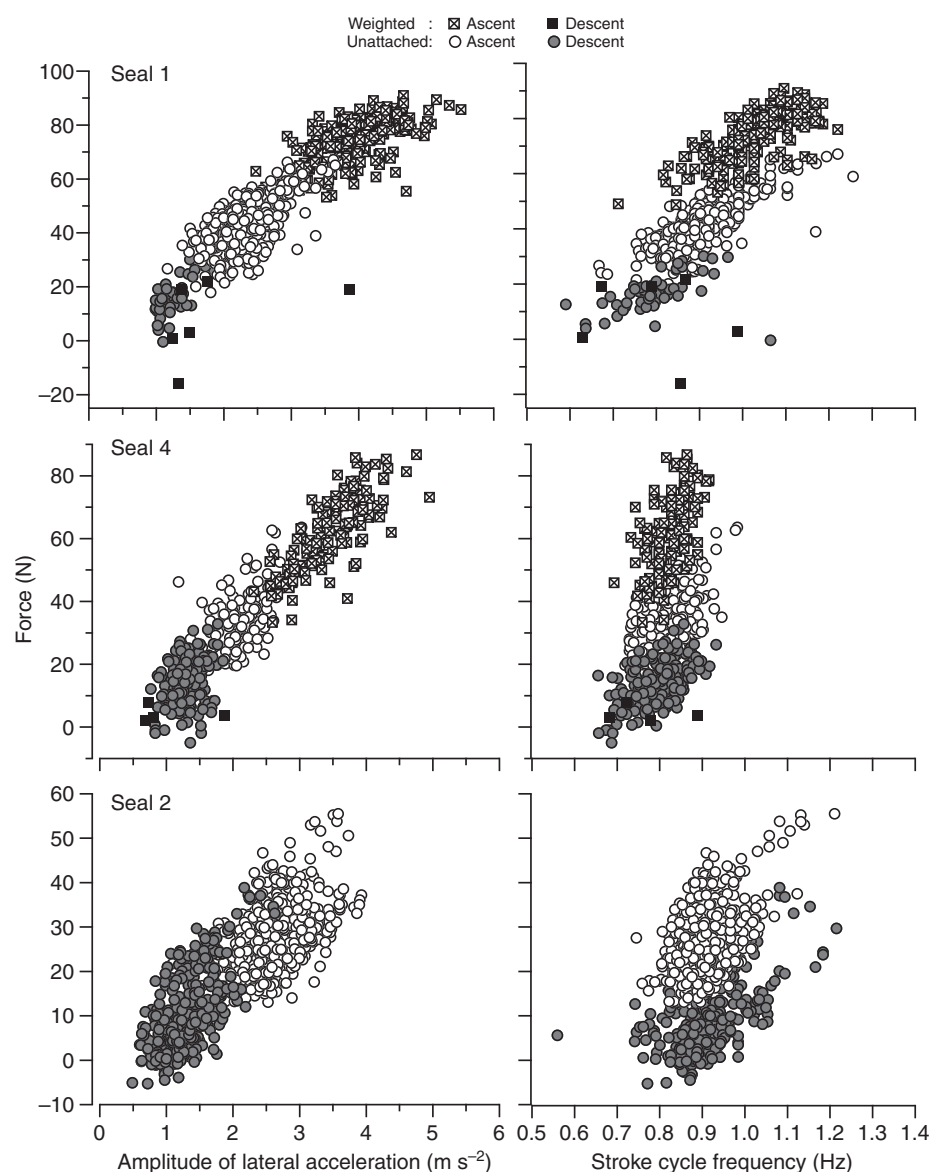
Fig. 5. Resistance force, including drag and buoyancy, during active swimming *vs* the amplitude of lateral acceleration and stroke cycle frequency. The active drag was assumed to be equal to the passive drag in these figures.

a slightly greater degree of head-up orientation during drift dives. We did not assess the estimated body density in relation to postural changes because we only recorded 14 drift dives, but the relatively large variation in body density estimated from the drift model may arise from changes in the drag coefficient during drift dives that are caused by postural differences.

For both the prolonged-glide and glide models, the drag coefficients used in the body density model were measured from horizontal glides (Bilo and Nachtigall, 1980). We expect that induced drag generated by lift-producing organs that help the animal maintain a non-vertical posture and direction of movement should influence the forces acting on the animal during non-vertical glides. If so, our estimate of the drag coefficient from horizontal glides, ignoring the effects of induced drag, may be an overestimate of body drag. At the same time, induced drag is expected to be generated during any glides or prolonged glides that are not perfectly vertical. In fact, the glides and prolonged glides we used to estimate body density had a mean pitch of 47.3±11.9 and 45.3±7.9 deg, respectively.

Estimated body density matched very closely density estimates from the isotope dilution method, ignoring the effects of lift-induced drag (Table 2). That result suggests that the magnitude of induced drag during horizontal and more vertical glides was small and/or that the effect of ignoring induced drag during horizontal glides is partly cancelled by also ignoring induced drag during the steeper 'vertical' glides, which in fact deviated from a perfectly vertical orientation. However, in the one case where we were able to make an estimate of induced drag, the floated condition in seal 2, the estimated corrected drag coefficient was 65–78% of the drag coefficient calculated from horizontal glides (see Appendix), indicating that our calculation using horizontal glides was an overestimation of the drag coefficient. But, using the adjusted drag coefficient did not make much difference to the agreement with the body density estimated from isotope dilution method (glide model, pre-adjustment $+1.4\,\mathrm{kg\,m^{-3}}$, adjustment $-2.1\,\mathrm{kg\,m^{-3}}$; prolonged-glide model, pre-adjustment $+2.3\,\mathrm{kg\,m^{-3}}$, adjustment $-1.6\,\mathrm{kg\,m^{-3}}$; residual in Table 2). Further research describing the lift-producing mechanisms in diving seals is required to better predict levels of

Table 5. Required logging parameters and conditions for three hydrodynamic models

Models	Logging parameters[a,b]	Condition[a]
Drift model	Depth (>100 m)	Drift dives
Prolonged-glide model	Depth (>100 m) Acceleration[c] (|Pitch| >30 deg) Swim speed	Prolonged-glides (reaching terminal speed)
Glide model[d]	Depth (>100 m) Acceleration[c] (|Pitch| >30 deg) Swim speed	(Stable) glides

[a]Parentheses show criteria for analysis in this study.
[b]Seawater density is not a necessary logging parameter but better provides an estimation of body density in all models if it is recorded.
[c]Pitch is calculated from longitudinal acceleration (see Materials and methods). To extract 'prolonged-glides or glides', acceleration of the axis which is oscillated during thrust production is also required
[d]The glide model can also be applied for prolonged-glides.

induced drag, which could improve body density estimation in free-swimming animals.

Advantages and disadvantages of the different hydrodynamic models

The analyzing criteria, necessary variables and required behaviours needed for the three methods to estimate body density using hydrodynamic performance models are presented in Table 5. The simplest method is the drift model, because this model requires only dive time *vs* depth profiles as recorded by data logging and telemetry instruments. However, to our knowledge, only a few species including elephant seals exhibit drift dives [e.g. New Zealand sea lions (Crocker et al., 2001a), sperm whales (Miller et al., 2008) and New Zealand fur seals (Page et al., 2005)], which limits its applicability to many species. In contrast, common stroking patterns (i.e. prolonged-glide and stroke-and-glide) have been observed across a wide taxonomic range, including cetaceans, pinnipeds, sea turtles and sea birds (e.g. Williams et al., 2000; Sato et al., 2003; Miller et al., 2004; Watanuki et al., 2005; Watanabe et al., 2006; Hays et al., 2007). Therefore, the methods using prolonged-glide and glide models are potentially applicable to a wider range of species compared with methods using the drift-dive model.

The prolonged-glide model requires that terminal speed be represented by a constant speed. We predicted the time required to reach terminal speed using measured body densities. The time to reach theoretical terminal speed increases as the density difference between the animal and the surrounding water decreases, so terminal speed can be more readily measured when body density differs from that of seawater. Although aquatic animals usually swim at $1–2\,\mathrm{m\,s^{-1}}$ during descent and ascent (e.g. Sato et al., 2007), the theoretical terminal speed of neutrally buoyant animals is zero, essentially making terminal speed unavailable as an estimator. However, animals rarely remain in a state of neutral buoyancy for long (Biuw et al., 2007; Robinson et al., 2010), as even small changes in body density would lead to substantial changes in the forces acting on the animal.

The glide model can be applied irrespective of the body density of the animals if stable glides of several seconds duration are recorded. The model assumes that only the combined forces of drag and buoyancy cause deceleration or acceleration during glides. However, rapid maneuvers of the animals or manipulations of body drag by the animal would violate that assumption. Although we might expect that animals will typically glide in an efficient manner to reduce locomotion costs, it is important to inspect body posture during glides to exclude unstable glides. In addition, the glide model requires accurate and frequent measures of swim speed because acceleration and deceleration during glides are based on relatively short-term changes in swim speeds.

Changes in stroking patterns resulting from body density manipulations

Our experiment clearly showed that changes in body density affected stroke rate and the proportion of time gliding. We simulated a reduction of body lipid by increasing the body density by attaching a lead weight to seals 1 and 4. The increased density caused the descent stroke rate to decrease and the ascent stroke rate to increase. Watanabe et al. reported similar results: descent stroke rate was lower during the weighted condition compared with the unattached condition whereas ascent stroke rate was higher in the weighted condition compared with the unattached condition (Watanabe et al., 2006). We also simulated increased fat content by attaching a float. When the lead weight was detached from the seal that was initially in the floated-and-weighted condition (seal 2), its descent stroke rate increased and the ascent stroke rate decreased.

The amplitude of lateral acceleration positively correlated with the resistance force caused by drag and buoyancy, suggesting that our animals adjusted the stroke intensity in response to changes in resistant force. In general, muscle fibers have their highest power output and efficiency over a relatively narrow range of contraction speeds and loads (Hill, 1950; Hill, 1964; Lovvorn et al., 1999). Therefore, it is possible that swim speed could be altered to bring about compensatory changes in thrust force against drag and buoyancy, thereby conserving thrust stroke force (supplementary material Fig. S2). For example, in case of seal 1, mean speed at ascent was $1.50\,\mathrm{m\,s^{-1}}$, which required an 87N propulsive force (see Materials and methods, Stroking patterns for the calculation; supplementary material Fig. S2). If the seal conserved the thrust force (i.e. 87N) irrespective of buoyancy, swim speed in the unattached state would have become faster because release of the lead weight dramatically lowered buoyancy resistance (expected speed, $2.1\,\mathrm{m\,s^{-2}}$; supplementary material Fig. S2). During descent, swim speed at both conditions would also become faster because buoyancy aids the seal's swimming (expected speed, $2.6\,\mathrm{m\,s^{-1}}$ for unattached and $3.0\,\mathrm{m\,s^{-1}}$ for weighted; supplementary material Fig. S2). However, the seals usually swam at $1–1.5\,\mathrm{m\,s^{-1}}$ during active stroking in all conditions (Fig. 4). We suggest that the seals adjusted propulsive force to maintain swim speed within a narrow range, despite changes in

buoyancy. Studies of swim speed scaling in aquatic animals have concluded that optimal swim speed is independent of the buoyancy of the animal, but is dependent on drag and metabolic rate (Sato et al., 2010; Watanabe et al., 2011). The seals in our study changed their stroke cycle frequency and stroke intensity (acceleration amplitude) to maintain forward speed in changing buoyancy conditions. Thus, it appears likely that they swam using a diverse range of Strouhal numbers (Taylor et al., 2003), with higher Strouhal numbers employed when swimming against greater resistant forces.

The amplitude of lateral acceleration positively correlated with resistance force overcome in active swimming (propulsive force) for all three seals, whereas stroke cycle frequency was positively correlated with force in two seals but not in the third (Fig. 5). Partial r^2 values were also consistently higher for the amplitude of lateral acceleration than for stroke cycle frequency (Table 4). There is little agreement whether changing stroke cycle frequency and/or stroke amplitude in seals alters thrust forces. Variation in stroke amplitude has been found in other air-breathing divers, such as penguins, sea turtles and dolphins (Skrovan et al., 1999; Wilson and Liebsch, 2003; Hays et al., 2007), but it is also well established that major fishes, and some captive dolphins and seals, modulate only stroking frequency (not amplitude) to swim faster (e.g. Fish, 1988; Fish, 1993; Videler and Wardle, 1991). We measured stroke cycle frequency and the amplitude of lateral acceleration, not stroke amplitude directly. If the horizontal oscillation of the hind flippers acts as a harmonic oscillator (e.g. Pabst, 1996), the displacement amplitude of the stroke (D) should follow a sinusoidal pattern that can be easily calculated from the amplitude of lateral acceleration (a_{LAT}) as $D=a_{LAT}/\omega^2$, where $\omega=2\pi f$ (angular velocity) and f is stroke cycle frequency. As a result, our seals might modulate stroke amplitude in response to changes in propulsive force but not necessarily in precisely the way predicted for a harmonic oscillator. To be effective, the back and flippers of seals must be highly damped because they function to produce thrust. Because dynamic acceleration is easy to measure with small low-power devices, we suggest a fruitful avenue for future research would be to relate the amplitude of stroke-induced lateral acceleration with simultaneous measurements of stroke amplitude and speed across a wide range of species.

CONCLUSIONS

Our results show remarkably good agreement between body density estimates obtained from body composition analysis and all three methods of analyzing gliding performance. Experimental manipulation of body density from programmed release of the weights and/or float were well tracked by the hydrodynamic methods, suggesting that all three methods have the potential to be applied as a powerful approach to tracking changes in body condition of a wide range of freely diving animals. This approach has much promise for exploring the influence of buoyancy on the behaviour and energetics of diving animals, as well as tracking their changes in relative body composition over time (Biuw et al., 2007; Robinson et al., 2010). Further refinement and application of this approach is of crucial importance for linking studies of animal movement and foraging ecology of marine predators to studies of their reproductive performance. These links are, in turn, essential for understanding how population dynamics can be affected by variations in behaviour and performance of animals (Morales et al., 2010), regardless of whether such variations are due to internal individual factors or external factors such as environmental change.

APPENDIX
The influence of lift during glides

A gliding seal may produce lift to maintain a non-vertical pitch, which should generate induced drag F_{Di}. Formal inclusion of any influence of lift should improve the accuracy of the prolonged-glide and glide models (Watanabe et al., 2006) (for details see Materials and methods, Body density models), but this is made difficult because of the lack of detailed information on the mechanics of how seals produce lift. Here we attempt to predict the influence of induced drag as a function of pitch using the prolonged-glide model.

First, we estimated body density using periods with steep pitch ($|\theta|>45$ deg), because the prolonged-glide model might underestimate the body density of animals at shallow pitch ($|\theta|\leq45$ deg) because of increasing induced drag (Watanabe et al., 2006). We then recorded the maximum speed for each prolonged glide and calculated the theoretical terminal speed using measured pitch. Residuals, calculated by subtracting the measured speed from the theoretical terminal speed, were plotted against measured pitch. Because lift increases with decreasing pitch, the residuals should negatively correlate with measured pitch. We consider the effects of induced drag at various pitches as the slope of the linear regression line of the residual vs pitch. The induced drag F_{Di} of a wing is calculated using the equation:

$$F_{Di} = \frac{2\kappa_{induced} F_L^2}{\pi\rho_{sw} R_A A_{plan} U^2} \ , \qquad (A1)$$

where F_L (N) is lift force ($F_L=F_B\cos\theta$), $\kappa_{induced}$ is an induced drag factor, R_A is aspect ratio and A_{plan} is the area of the wing (Alexander, 2003). Because we do not know the values for all of the terms in Eqn A1 for elephant seals, we combined $\kappa_{induced}/\pi\rho_{sw}R_A A_{plan}$ into an unknown variable X. We estimated X when the coefficient of the slope of the model residuals regressed against pitch was close to zero.

A term for induced drag is included during horizontal glides: $F_D+F_{Di}=ma$. We calculated the drag coefficient minus induced drag $C_{d,fn}$ by combining Eqn 13 (see Materials and methods) with Eqn A1:

$$C_{d,fn} = C_{d,f} - 4XF_B^2\cos^2\theta_h / (A_f\rho_{sw,h}U_h^4), \qquad (A2)$$

where U_h, θ_h and $\rho_{sw,h}$ are mean values of speed, pitch and density of seawater during horizontal glides, respectively.

A new equation including the effect of lift for the prolonged-glide model is given by: $F_B\sin\theta=F_D+F_{Di}$. Theoretical terminal speed U_{ter} is therefore:

$$U_{ter}^2 = \frac{F_B\sin\theta + \sqrt{F_B^2\sin^2\theta - 4C_{d,fn}\rho_{sw}A_f \cdot XF_B^2\cos^2\theta}}{C_{d,fn}\rho_{sw}A_f} \ . \qquad (A3)$$

We fitted this model as we described previously (see Materials and methods, Body density models). ρ_{seal} and $C_{d,fn}$ were estimated at the same time by the least-squares method for each dive.

We also re-estimated body density using the glide model. A term for induced drag is included during a glide: $ma=F_B\sin\theta-(F_D+F_{Di})$. Thus, the theoretical acceleration of the new equation is calculated by:

$$a = -\frac{C_{d,fn}A_f}{m}0.5\rho_{sw}U^2 + (\rho_{sw}/\rho_{seal}-1)g\sin\theta$$
$$-\frac{2X}{mU^2}F_B^2\cos^2\theta \ . \qquad (A4)$$

We selected glides using the same criteria as described in the Materials and methods, Body density models. ρ_{seal} and $C_{d,fn}$ were

estimated by the non-linear least-squares method at each condition for each animal.

We were able to quantify the influence of lift as the coefficient of the slope only for seal 2 in the floated condition (r^2=0.57, $F_{1,42}$=55.68, P<0.001). In all other cases, we did not obtain a statistically significant value of the slope (seal 1, weighted, r^2=0.16, $F_{1,12}$=2.27, P=0.16; unattached, r^2=0.0070, $F_{1,36}$=0.25, P=0.62; seal 2, floated-and-weighted, r^2=0.12 $F_{1,17}$=0.033, P=0.858; unattached, r^2=0.0012, $F_{1,7}$=0.0091, P=0.93; seal 4, weighted, $F_{1,24}$=0.029, r^2=0.0012, P=0.87). Insufficient glide data were obtained from the unattached condition for seal 4. We therefore re-estimated the body density in only the floated condition for seal 2. The estimated density was 1017.5 kg m^{-3} for the glide model and 1017.0 kg m^{-3} for the prolonged-glide model, and increased by only 0.35% for the glide model and 0.39% for the prolonged-glide model (Table 2). The re-calculated drag coefficient was 0.15±0.005 (N=76 glides) for the glide model and 0.18±0.007 (N=34 dives) for the prolonged-glide model. The sum of squared residuals of the glide model using lift-adjusted drag coefficients (0.01238) was less than half of the pre-adjustment residual of the glide model (0.02987), indicating a somewhat better model fit for the data when the influence of lift could be estimated.

LIST OF SYMBOLS AND ABBREVIATIONS

a	acceleration
A	frontal or surface area of the seal
A_f	frontal area of the seal
a_{LAT}	amplitude of the lateral dynamic acceleration
A_{plan}	area of the wing
A_S	surface area of the seal
C_d	drag coefficient
$C_{d,f}$	drag coefficient based on frontal area
$C_{d,fn}$	drag coefficient based on frontal area minus induced drag
$C_{d,s}$	drag coefficient based on total surface area
D	stroke amplitude of the hind-flipper
f	stroke cycle frequency of the hind-flipper
F_B	buoyancy force
F_D	drag force
F_{Di}	induced drag force
F_L	lift force
F_R	resistance force
$\mathbf{g}$	gravity
L	standard length of the seal
m	total body mass of the seal, calculated by $m_{seal}m_e$
$m_{attachment}$	mass of a lead weight and/or the float
m_e	multiplier for entrained water adhering to the surface of the seal
m_{seal}	body mass of the seal
P_a	proportion of total amount of the ash to body mass
P_{bw}	proportion of total amount of the body water to body mass
P_l	proportion of total amount of the lipid to body mass
P_p	proportion of total amount of the protein to body mass
R_A	aspect ratio
Re	Reynolds number
TBA	total body ash
TBL	total body lipid
TBP	total body protein
TBW	total body water
U	swim speed
U_{drift}	theoretical drift rate
U_h	swim speed during horizontal glide
U_{ter}	theoretical terminal speed
$V_{attachment}$	volume of a lead weight and/or the float
V_{seal}	volume of the seal
X	combined $\kappa_{induced}/\pi\rho_{sw}R_A A_{plan}$ as an unknown variable
λ	active-to-passive drag ratio
$\kappa_{induced}$	induced drag factor
ν	kinematic viscosity of seawater
θ	pitch angle
θ_h	pitch angle during horizontal glide
ρ_a	density of the ash
ρ_{bw}	density of the body water
ρ_l	density of the lipid
ρ_p	density of the protein
ρ_{seal}	density of the seal
$\rho_{seal, manipulation}$	density of the seal for each buoyancy manipulation condition
ρ_{sw}	density of seawater
$\rho_{sw,h}$	density of seawater during horizontal glide
ω	angular velocity

REFERENCES

Alexander, R. M. (1999). One price to run, swim or fly? *Nature* **397**, 651-653.

Alexander, R. M. (2003). *Principles of Animal Locomotion*. Princeton, NJ: Princeton University Press.

Anderson, S. A., Costa, D. P. and Fedak, M. A. (1993). Bioenergetics. In *Antarctic Pinnipeds: Research Methods and Techniques* (ed. R. Laws), pp. 291-315. Cambridge: Cambridge University Press.

Arnbom, T., Fedak, M. A., Boyd, I. L. and McConnell, B. J. (1993). Variation in weaning mass of pups in relation to maternal mass, postweaning fast duration, and weaned pup behaviour in southern elephant seals (*Mirounga leonina*) at south Georgia. *Can. J. Zool.* **71**, 1772-1781.

Arnbom, T., Fedak, M. A. and Boyd, I. L. (1997). Factors affecting maternal expenditure in southern elephant seals during lactation. *Ecology* **78**, 471-483.

Arnould, J. P. Y. (1995). Indices of body condition and body composition in female antarctic fur seals (*Arctocephalus gazella*). *Mar. Mamm. Sci.* **11**, 301-313.

Arnould, J. P. Y., Boyd, I. L. and Speakman, J. R. (1996). Measuring the body composition of Antarctic fur seals (*Arctocephalus gazella*): validation of hydrogen isotope dilution. *Physiol. Zool.* **69**, 93-116.

Austin, D., Bowen, W. D., McMillan, J. I. and Boness, D. J. (2006). Stomach temperature telemetry reveals temporal patterns of foraging success in a free-ranging marine mammal. *J. Anim. Ecol.* **75**, 408-420.

Bailleul, F., Pinaud, D., Hindell, M., Charrassin, J. B. and Guinet, C. (2008). Assessment of scale-dependent foraging behaviour in southern elephant seals incorporating the vertical dimension: a development of the first passage time method. *J. Anim. Ecol.* **77**, 948-957.

Barrett, D. S., Triantafyllou, M. S. and Yue, D. K. P. (1999). Drag reduction in fishlike locomotion. *J. Fluid Mech.* **392**, 183-212.

Beck, C. A., Bowen, W. D. and Iverson, S. J. (2000). Seasonal changes in buoyancy and diving behaviour of adult grey seals. *J. Exp. Biol.* **203**, 2323-2330.

Bell, C. M., Hindell, M. A. and Burton, H. R. (1997). Estimation of body mass in the southern elephant seal, *Mirounga leonina*, by photogrammetry and morphometrics. *Mar. Mamm. Sci.* **13**, 669-682.

Bilo, D. and Nachtigall, W. (1980). A simple method to determine drag coefficients in aquatic animals. *J. Exp. Biol.* **87**, 357-359.

Biuw, M., McConnell, B., Bradshaw, C. J. A., Burton, H. and Fedak, M. A. (2003). Blubber and buoyancy: monitoring the body condition of free-ranging seals using simple dive characteristics. *J. Exp. Biol.* **206**, 3405-3423.

Biuw, M., Boehme, L., Guinet, C., Hindell, M., Costa, D., Charrassin, J. B., Roquet, F., Bailleul, F., Meredith, M., Thorpe, S. et al. (2007). Variations in behavior and condition of a Southern Ocean top predator in relation to *in situ* oceanographic conditions. *Proc. Natl. Acad. Sci. USA* **104**, 13705-13710.

Borazjani, I. and Sotiropoulos, F. (2008). Numerical investigation of the hydrodynamics of carangiform swimming in the transitional and inertial flow regimes. *J. Exp. Biol.* **211**, 1541-1558.

Bowen, W. D. and Iverson, S. J. (1998). Estimation of total body water in pinnipeds using hydrogen-isotope dilution. *Physiol. Zool.* **71**, 329-332.

Costa, D. P. (1987). Isotopic methods for quantifying material and energy intake of free-ranging marine mammals. In *Approaches to Marine Mammal Energetics* (ed. A. C. Huntley, D. P. Costa, G. A. J. Worthy and M. A. Castellini), pp. 43-66. Lawrence, KS: Allen Press.

Costa, D. P. (1993). The relationship between reproductive and foraging energetics and the evolution of the Pinnipedia. In *Marine Mammals: Advances in Behavioural and Population Biology* (ed. I. L. Boyd), pp. 293-314. Oxford: Symposium Zoological Society of London, Oxford University Press.

Costa, D. P., Le Boeuf, B. J., Huntley, A. C. and Ortiz, C. L. (1986). The energetics of lactation in the northern elephant seal, *Mirounga angustirostris*. *J. Zool.* **209**, 21-34.

Crocker, D. E. (1995). Reproductive effort and fasting physiology of female northern elephant seals, *Mirounga angustirostris*. PhD thesis, University of California Santa Cruz, Santa Cruz, CA, USA.

Crocker, D. E., Le Boeuf, B. J. and Costa, D. P. (1997). Drift diving in female northern elephant seals, Implications for food processing. *Can. J. Zool.* **75**, 27-39.

Crocker, D. E., Gales, N. J. and Costa, D. P. (2001a). Swimming speed and foraging strategies of New Zealand sea lions (*Phocarctos hookeri*). *J. Zool.* **254**, 267-277.

Crocker, D. E., Williams, J. D., Costa, D. R. and Le Boeuf, B. J. (2001b). Maternal traits and reproductive effort in northern elephant seals. *Ecology* **82**, 3541-3555.

Fauchald, P. and Tveraa, T. (2003). Using first-passage time in the analysis of area-restricted search and habitat selection. *Ecology* **84**, 282-288.

Fedak, M. A., Arnbom, T., McConnell, B. J., Chambers, C., Boyd, I. L., Harwood, J. and McCann, T. S. (1994). Expenditure, investment, and acquisition of energy in southern elephant seals. In *Elephant Seals: Population Ecology, Behavior and Physiology* (ed. B. J. Le Boeuf and R. M. Laws), pp. 354-373. Berkeley: University of California Press.

Fedak, M. A., Arnbom, T. and Boyd, I. L. (1996). The relation between the size of southern elephant seal mothers, the growth of their pups, and the use of maternal energy, fat, and protein during lactation. *Physiol. Zool.* **69**, 887-911.

Feldkamp, S. D. (1987). Swimming in the California sea lion: morphometrics, drag and energetics. *J. Exp. Biol.* **131**, 117-135.

Fields, D. A., Higgins, P. B. and Radley, D. (2005). Air-displacement plethysmography, here to stay. *Curr. Opin. Clin. Nutr. Metab. Care* **8**, 624-629.

Fish, F. E. (1988). Kinematics and estimated thrust production of swimming harp and ringed seals. *J. Exp. Biol.* **137**, 157-173.

Fish, F. E. (1993). Power output and propulsive efficiency of swimming bottlenose dolphins (*Tursiops truncatus*). *J. Exp. Biol.* **185**, 179-193.

Fox, J. (2002). *An R and S-Plus Companion to Applied Regression.* London: Sage Publications.

Hall, A. J., McConnell, B. J. and Barker, R. J. (2001). Factors affecting first-year survival in grey seals and their implications for life history strategy. *J. Anim. Ecol.* **70**, 138-149.

Hays, G. C., Marshall, G. J. and Seminoff, J. A. (2007). Flipper beat frequency and amplitude changes in diving green turtles, *Chelonia mydas. Mar. Biol.* **150**, 1003-1009.

Hill, A. V. (1950). The dimensions of animals and their muscular dynamics. *Sci. Prog.* **38**, 209-230.

Hill, A. V. (1964). The efficiency of mechanical power development during muscular shortening and its relation to load. *Proc. R. Soc. Lond. B* **159**, 319-324.

Hind, A. T. and Gurney, W. S. C. (1997). The metabolic cost of swimming in marine homeotherms. *J. Exp. Biol.* **200**, 531-542.

Jonsen, I. D., Flemming, J. M. and Myers, R. A. (2005). Robust state-space modeling of animal movement data. *Ecology* **86**, 2874-2880.

Kuhn, C. E., Crocker, D. E., Tremblay, Y. and Costa, D. P. (2008). Time to eat, measurements of feeding behaviour in a large marine predator, the northern elephant seal *Mirounga angustirostris. J. Anim. Ecol.* **78**, 513-523.

Le Boeuf, B. J., Costa, D. P., Huntley, A. C. and Feldkamp, S. D. (1988). Continuous deep diving in female northern elephant seals. *Can. J. Zool.* **66**, 446-458.

Le Boeuf, B. J., Crocker, D. E., Costa, D. P., Blackwell, S. B., Webb, P. M. and Houser, D. S. (2000). Foraging ecology of northern elephant seals. *Ecol. Monogr.* **70**, 353-382.

Lide, D. R. (2003). *Handbook of Chemistry and Physics* (84th edn). Boca Raton: CRC Press.

Lovvorn, J. R. and Jones, D. R. (1991). Effects of body size, body fat and change in pressure with depth on buoyancy and costs of diving in ducks. *Can. J. Zool.* **69**, 2879-2887.

Lovvorn, J. R., Croll, D. A. and Liggins, G. A. (1999). Mechanical *versus* physiological determinants of swimming speeds in diving Brünnich's guillemots. *J. Exp. Biol.* **202**, 1741-1752.

Lovvorn, J. R., Watanuki, Y., Kato, A., Naito, Y. and Liggins, G. A. (2004). Stroke patterns and regulation of swim speed and energy cost in free-ranging Brünnich's guillemots. *J. Exp. Biol.* **207**, 4679-4695.

Lukaski, H. C. (1987). Methods for the assessment of human-body composition – traditional and new. *Am. J. Clin. Nutr.* **46**, 537-556.

McMahon, C. R., Burton, H. R. and Bester, M. N. (2000). Weaning mass and the future survival of juvenile southern elephant seals, *Mirounga leonina*, at Macquarie Island. *Antarct. Sci.* **12**, 149-153.

Miller, P. J. O., Johnson, M. P., Tyack, P. L. and Terray, E. A. (2004). Swimming gaits, passive drag and buoyancy of diving sperm whales *Physeter macrocephalus. J. Exp. Biol.* **207**, 1953-1967.

Miller, P. J. O., Aoki, K., Rendell, L. E. and Amano, M. (2008). Stereotypical resting behavior of the sperm whale. *Curr. Biol.* **18**, R21-R23.

Mitani, Y., Andrews, R. D., Sato, K., Kato, A., Naito, Y. and Costa, D. P. (2009). Three-dimensional resting behaviour of northern elephant seals, drifting like a falling leaf. *Biol. Lett.* **6**, 163-166.

Moore, F. D., Olsen, K. H., McMurray, J. D., Parker, H. V., Ball, M. R. and Boyden, C. M. (1963). *The Body Cell Mass and its Supporting Environment: Body Composition in Health and Disease.* Philadelphia, PA: W. B. Saunders.

Morales, J. M., Moorcroft, P. R., Matthiopoulos, J., Frair, J. L., Kie, J. G., Powell, R. A., Merril, E. H. and Haydon, D. T. (2010). Building the bridge between animal movement and population dynamics. *Philos. Trans. R. Soc. Lond. B* **365**, 2289-2301.

Mori, Y. (1998). The optimal patch use in divers, optimal time budget and the number of dive cycles during bout. *J. Theor. Biol.* **190**, 187-199.

Moya-Laraño, J., Macías-Ordóñez, R., Blanckenhorn, W. U. and Fernández-Montraveta, C. (2008). Analysing body condition, mass, volume or density? *J. Anim. Ecol.* **77**, 1099-1108.

Oliver, G. W., Morris, P. A., Thorson, P. H. and Le Boeuf, B. J. (1998). Homing behavior of juvenile northern elephant seals. *Mar. Mamm. Sci.* **14**, 245-256.

Ortiz, C. L., Costa, D. P. and Le Boeuf, B. J. (1978). Water and energy flux in elephant seal pups fasting under natural conditions. *Physiol. Zool.* **51**, 166-178.

Pabst, D. A. (1996). Springs in swimming animals. *Am. Zool.* **36**, 723-735.

Pace, N. and Rathbun, E. N. (1945). Studies on body composition III. The body water and chemically combines nitrogen content in relation to fat content. *J. Biol. Chem.* **158**, 685-691.

Page, B., McKenzie, J. and Goldsworthy, S. D. (2005). Dietary resource partitioning among sympatric New Zealand and Australian fur seals. *Mar. Ecol. Prog. Ser.* **293**, 283-302.

Patterson, T. A., Thomas, L., Wilcox, C., Ovaskainen, O. and Matthiopoulos, J. (2008). State-space models of individual movement. *Trends Ecol. Evol.* **23**, 87-94.

Pomeroy, P. P., Fedak, M. A., Anderson, S. S. and Rothery, P. (1999). Consequences of maternal size for reproductive expenditure and pupping success of grey seals at North Rona, Scotland. *J. Anim. Ecol.* **68**, 235-253.

Reilly, J. J. and Fedak, M. A. (1990). Measurement of the body composition of living gray seals by hydrogen isotope dilution. *J. Appl. Physiol.* **69**, 885-891.

Robinson, P. W., Tremblay, Y., Crocker, D. E., Kappes, M. A., Kuhn, C. E., Shaffer, S. A., Simmons, S. E. and Costa, D. P. (2007). A comparison of indirect measures of feeding behaviour based on ARGOS tracking data. *Deep Sea Res. Part II* **54**, 356-368.

Robinson, P. W., Simmons, S. E., Crocker, D. E. and Costa, D. P. (2010). Measurements of foraging success in a highly pelagic marine predator, the northern elephant seal. *J. Anim. Ecol.* **79**, 1146-1156.

Sakamoto, K. Q., Sato, K., Ishizuka, M., Watanuki, Y., Takahashi, A., Daunt, F. and Wanless, S. (2009). Can ethograms be automatically generated using body acceleration data from free-ranging birds? *PLoS ONE* **4**, e5379.

Sato, K., Mitani, Y., Cameron, M. F., Siniff, D. B. and Naito, Y. (2003). Factors affecting stroking patterns and body angle in diving Weddell seals under natural conditions. *J. Exp. Biol.* **206**, 1461-1470.

Sato, K., Watanuki, Y., Takahashi, A., Miller, P. J. O., Tanaka, H., Kawabe, R., Ponganis, P. J., Handrich, Y., Akamatsu, T., Watanabe, Y. et al. (2007). Stroke frequency, but not swimming speed, is related to body size in free-ranging seabirds, pinnipeds and cetaceans. *Proc. R. Soc. Lond. B* **274**, 471-477.

Sato, K., Shiomi, K., Watanabe, Y., Watanuki, Y., Takahashi, A. and Ponganis, P. J. (2010). Scaling of swim speed and stroke frequency in geometrically similar penguins: they swim optimally to minimize cost of transport. *Proc. R. Soc. Lond. B* **277**, 707-714.

Skrovan, R. C., Williams, T. M., Berry, P. S., Moore, P. W. and Davis, R. W. (1999). The diving physiology of bottlenose dolphins (*Tursiops truncatus*) II. Biomechanics and changes in buoyancy at depth. *J. Exp. Biol.* **202**, 2479-2761.

Suzuki, I., Naito, Y., Folkow, L. P., Miyazaki, N. and Blix, A. S. (2009). Validation of a device for accurate timing of feeding events in marine animals. *Polar Biol.* **32**, 667-671.

Taylor, G. K., Nudds, R. L. and Thomas, A. L. (2003). Flying and swimming animals cruise at a Strouhal number tuned for high power efficiency. *Nature* **425**, 707-711.

Thompson, D., Hiby, A. R. and Fedak, M. A. (1993). How fast should I swim? Behavioural implications of diving physiology. *Symp. Zool. Soc. Lond.* **66**, 349-368.

Tremblay, Y., Roberts, A. J. and Costa, D. P. (2007). Fractal landscape method, an alternative approach to measuring area-restricted searching behavior. *J. Exp. Biol.* **210**, 935-945.

UNESCO (1981). *Tenth Report of the Joint Panel on Oceanographic Tables and Standards.* UNESCO Technical Papers in Marine Science, Vol. 36. Paris: UNESCO.

Videler, J. J. and Wardle, C. S. (1991). Fish swimming stride by stride: speed limits and endurance. *Rev. Fish Biol. Fish.* **1**, 23-40.

Vogel, S. (1994). *Life in Moving Fluids: The Physical Biology of Flow* (2nd edn). Princeton, NJ: Princeton University Press.

Watanabe, Y., Baranov, E. A., Sato, K., Naito, Y. and Miyazaki, N. (2006). Body density affects stroke patterns in Baikal seals. *J. Exp. Biol.* **209**, 3269-3280.

Watanabe, Y. Y., Sato, K., Watanuki, Y., Takahashi, A., Mitani, Y., Amano, M., Aoki, K., Narazaki, T., Iwata, T., Minamikawa, S. et al. (2011). Scaling of swim speed in breath-hold divers. *J. Anim. Ecol.* **80**, 57-68.

Watanuki, Y., Takahashi, A., Daunt, F., Wanless, S., Harris, M., Sato, K. and Naito, Y. (2005). Regulation of stroke and glide in a foot-propelled avian diver. *J. Exp. Biol.* **208**, 2207-2216.

Webb, P. M., Crocker, D. E., Blackwell, S. B., Costa, D. P. and Le Boeuf, B. J. (1998). Effects of buoyancy on the diving behaviour of northern elephant seals. *J. Exp. Biol.* **201**, 2349-2358.

Williams, T. M. and Kooyman, G. L. (1985). Swimming performance and hydrodynamic characteristics of harbor seals (*Phoca vitulina*). *Physiol. Zool.* **58**, 576-589.

Williams, T. M., Davis, R. W., Fuiman, L. A., Francis, J., Le Boeuf, B. J., Horning, M., Calambokidis, J. and Croll, D. A. (2000). Sink or swim: strategies for cost-efficient diving by marine mammals. *Science* **288**, 133-136.

Wilson, R. P. and Liebsch, N. (2003). Up-beat motion in swinging limbs, new insights into assessing movement in free-living aquatic vertebrates. *Mar. Biol.* **142**, 537-547.

Wilson, R. P., Grant, W. S. and Duffy, D. C. (1986). Recording devices on free-ranging marine animals: does measurement affect foraging performance? *Ecology* **67**, 1091-1093.

Wilson, R. P., Cooper, J. and Plötz, J. (1992). Can we determine when marine endotherm feed? A case study with seabirds. *J. Exp. Biol.* **167**, 267-275.

Wilson, R. P., White, C. R., Quintana, F., Halsey, L. G., Liebsch, N., Martin, G. R. and Butler, P. J. (2006). Moving towards acceleration for estimates of activity-specific metabolic rate in free-living animals: the case of the cormorant. *J. Anim. Ecol.* **75**, 1081-1090.